Supporting information

Rationally designed multifunctional hyperbranched polymer as a trace additive for stable zinc anodes

*Jiekai Hong[a], Zumin Chen[a], Xun Li[a], Kai Feng[b], and Jiye Luo [a]**

a J. Hong, Z. Chen, X. Li, Dr. J. Luo
School of Chemical Engineering and Light Industry
Guangdong University of Technology
Guangzhou 510006, China
E-mail: luojiye@gdut.edu.cn

b Dr. K. Feng
College of Chemistry & Engineering
Yantai University
Yantai 264005, China

Experimental section

Electrolyte and synthesis

Preparation of electrolyte: 2 M $ZnSO_4$ electrolyte was prepared using $ZnSO_4 \cdot 7H_2O$ and ultrapure water. Different amounts of N-HPG (Mn=2150) were added to the 2 M $ZnSO_4$ electrolyte to prepare electrolytes containing N-HPG at different concentrations. Full cell electrolytes were prepared in a similar way using 2 M $ZnSO_4$ + 0.2 M $MnSO_4$ salt as the base salt. $ZnSO_4 \cdot 7H_2O$ and $MnSO_4 \cdot H_2O$ were purchased from Aladdin Reagent Company and were used without any purification.

Synthesis of N-HPG: 224.4 mg of potassium tert-butoxide was loaded in a reaction flask under a nitrogen atmosphere. Subsequently, 758.15 mg of trimethyl epoxypropyl ammonium chloride in 0.5 mL of dimethyl sulfoxide was added into the flask. The mixture was heated to 60 °C with continuous stirring. Next, 3.704 g of 2,3-epoxypropanol was slowly injected into the flask, then the temperature was gradually increased to 120°C and kept for 24 h. After the reaction, the solvent was removed by vacuum evaporation and the hyperbranched polymer was obtained as a brown paste, which was used without further purification.

Synthesis of manganese dioxide: 2.37 g $KMnO_4$, 3.33 g $MnSO_4$ and 50 ml of deionized water were added in a 150 ml round-bottom flask. The mixture was stirred at room temperature to ensure thorough mixing. Subsequently, 10 mL of 6 mol/L nitric acid was added dropwisely. After the addition of nitric acid, the mixture was heated to 100°C and vigorous stirred for 24 hours. After the reaction, the product was filtered, washed with deionized water to neutral, and dried to yield a gray powder, which was identified as α-MnO_2. The SEM and XRD characterization results for MnO_2 are presented in Figures S19 and S20, respectively.

Material characterization

SEM measurements were conducted using a Phenom Prox microscope to characterize the morphology of the samples. The Raman spectroscopy was performed using a HORIBA Jobin Yvon LabRAM HR800 instrument with a laser wavelength of 633 nm. X-ray diffraction (XRD) analysis was conducted using a Rigaku SmartLab instrument with a scanning rate of 10°/min.

Electrochemical characterization

Interface morphology observation: The morphological changes at the zinc electrode interface during galvanization at a current density of 5 mA cm^{-2} were observed using a customized in-situ optical microscope integrated with a GAOPIN GP-300C commercial camera, which provides real-time visual data of the electrode surface.

Hydrogen evolution reaction (HER) tests: HER reactions were systematically evaluated using an electrochemical

workstation (CHI 760e) equipped with a three-electrode system, in which a platinum sheet, a graphite electrode, and a mercury/mercurous sulfate electrode (MSE) were used as the working, counter, and reference electrode, respectively.

Oxygen evolution reaction (OER) assessments: OER measurements were performed on a Zn//SS half-cell with the potential scanning from the open-circuit potential to the positive polarization limit at a scan rate of 1 mV s^{-1}.

Chronoamperometry (CA) measurements: CA measurements were performed using an electrochemical workstation (CHI 760e) with Zn foils (1 cm * 1 cm) as the working and counter electrodes, respectively, and a MSE electrode as the reference electrode. The measurements were carried out at an overpotential of -150 mV with a period of 3600 s.

Scanning electrochemical microscopy (SECM) charactrization: SECM scans were performed using a CHI 920d instrument with a constant voltage mode.

Electrochemical impedance spectroscopy (EIS): The impedance of Zn//Zn symmetric cells containing different electrolytes were measured using a DH7000C (DONGHUA) electrochemical workstation. The testing frequency range was 100 kHz to 0.1 Hz, with an AC voltage amplitude of 10 mV.

Ionic conductivity tests: The ionic conductivities of the electrolytes were measured at room temperature using the EIS method. SS//SS symmetric cells were used and the measurements were carried out on an Autolab PGSTAT302N instrument.

Galvanostatic measurements（GMs）: GMs were carried out using an electrochemical workstation (CHI 760e) with a three-electrode system. A platinum rotating disk electrode (Pt-RDE, PINE) with a diameter of 5 mm was employed as the working electrode. The counter electrode and the reference electrode were Zn bar and saturated mercury-mercurous sulfate electrode (SMSE), respectively. The volume of the electroplating solution was 50 ml and the temperature was controlled at 25°C. Before the GMs, a thin Znic layer was deposited on the Pt-RDE (10 mA cm^{-2}, 600 s) in the base electroplating solution to prepare a Zinc Rotating Disc (Zn-RDE). The GMs were carried out with the current density of 1 mA cm^{-2}. The rotating speed of the working electrode was controlled at 100 rpm or 1000 rpm to simulate the forced convection at zinc tips and zinc surfaces, respectively. At intervals of 600 seconds, 1200 seconds, and 1800 seconds, certain amount of N-HPG were introduced correspondingly and the potentials were continuously collected throughout the experimental procedure.

Battery testing

Cathode preparation: The cathodes were prepared by mixing the active material (MnO_2), conductive carbon black (Super P), and binder (PVDF) in a mass ratio of 7:2:1 using N-methyl-2 pyrrolideone (NMP) as the solvent. Then the resulting slurry was coated onto the carbon cloth (12 mm in diameter) with an MnO_2 loading of 0.8–1.2 mg cm^{-2}. The coated current

collectors were dried in a vacuum oven at 80°C for 12 hours.

Battery testing: The Zn//Zn, Zn//Cu, and Zn//MnO_2 batteries were assembled and tested in CR2025 coin-type cells under air atmosphere. Glass fiber separator (Whatman, GF/D) was used, the zinc foil thickness was 100 μm, and the electrolyte volume was 150 μL. Galvanostatic charge-discharge (GCD) testing and rate capability evaluation were performed using a LAND battery testing system.

DFT calculations and MD simulations

Density functional theory (DFT) calculations were carried out using the Quantum Espresso package,[1] employing the Perdew-Burke-Ernzerhof (PBE) parameterization,[2,3] for the exchange correlation functional within the generalized gradient approximation (GGA). Vanderbilt ultra-soft pseudopotentials were utilized, with electronic wave functions expanded in plane-waves using a kinetic energy cutoff of 30 Ry. Among densely packed zinc surfaces, the Zn (002) surface was identified as the most stable.[4] To model the surface, periodic supercells were employed, featuring an iron slab of 11×11 in-plane size to prevent interaction with periodic replicas of N-HPG, along with a 20 Å thick vacuum region. Brillouin zone sampling utilized a 2×2×1 Monkhorst Pack grid. For the zinc dendrite model, Wulff constructions (dominated by (101) and (100) surfaces) with an 8-layer stacked mode were employed. A N-HPG molecule was adsorbed on the two Zn substrates in their most stable configuration, and the system was relaxed under either a 0 eV/Å or 0.05 eV/Å electrostatic field.

Molecular dynamics (MD) simulations were performed using the large-scale atomic/molecular parallel simulator (LAMMPS) package.[5] Simulations included pure $ZnSO_4$ solution and a mixed sample of $ZnSO_4$ and N-HPG additive. The simulated box dimensions were 4.45×4.45×4.45 nm^3 with periodic boundary conditions, containing 130 $ZnSO_4$ and 2950 water molecules, and 130 $ZnSO_4$, 3 N-HPG, and 2872 H_2O molecules, respectively. The cell structure was constructed with PACKMOL software.[6] The force field of water molecules was modeled by SPC/E. The general Amber force field (GAFF) [7] was used to describe the N-HPG and SO_4^{2-} ions, Zn^{2+} parameters were taken from the work by Babu *et al*.[8] The annealing simulation from 798 K to 298 K was applied to our systems to speed up the energy relaxation. Subsequently, molecular dynamics simulations under NPT ensemble at 298 K and 1 atm were performed for 10 ns for each system. Based on the structure obtained from the previous step, the system was further relaxed at 298 K in the NVT ensemble for 10 ns to obtain the equilibrium structure. The data for the last 5 ns were used for analyses. The Nosé-Hoover thermostat [9] and the extended Lagrangian approach[10] were applied to control the temperature and pressure, respectively. After completing MD simulations, the radial distribution function was analyzed. A solvation structure of Zn^{2+} from output stable structure was extracted for calculating binding energy between Zn^{2+} and solvation molecules.

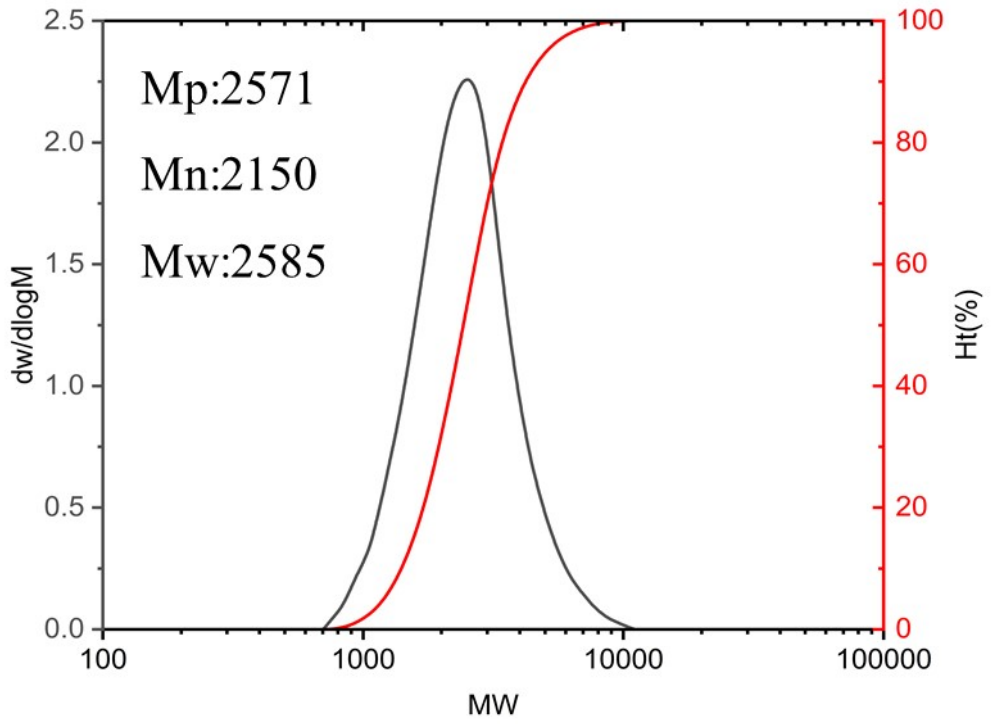

Fig. S1 GPC Data of N-HPG

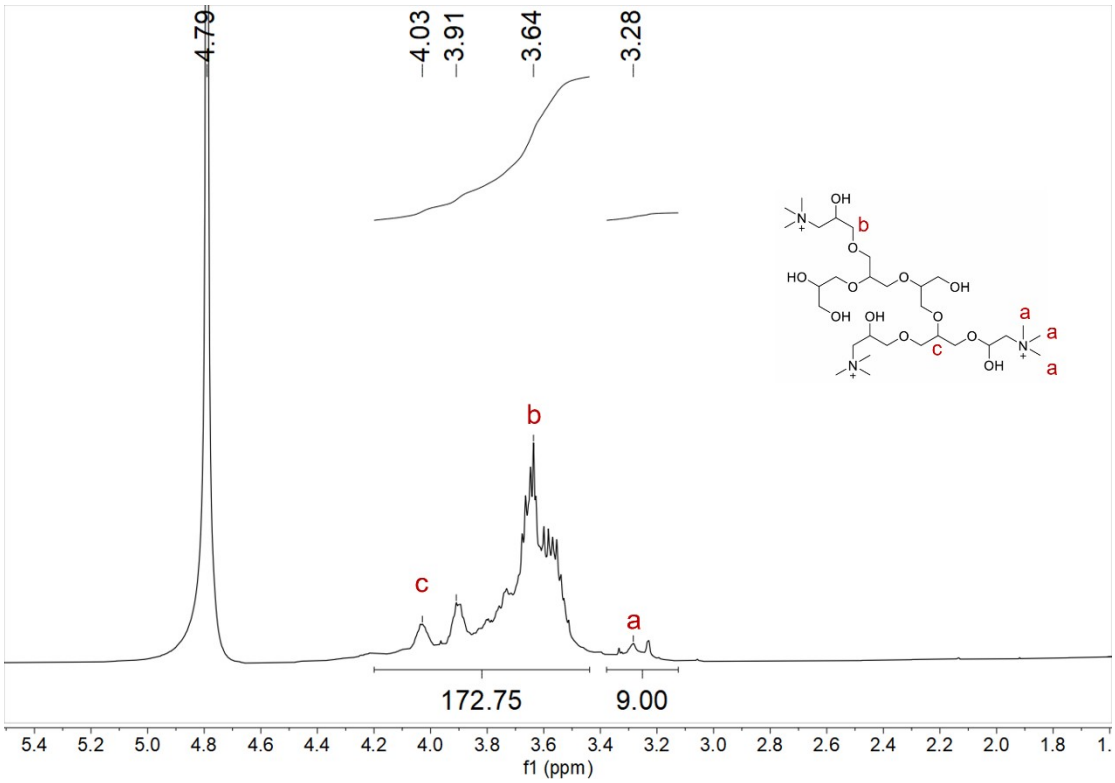

Fig. S2 ^{1}H NMR (D2O, 400 MHz) spectra of N-HPG

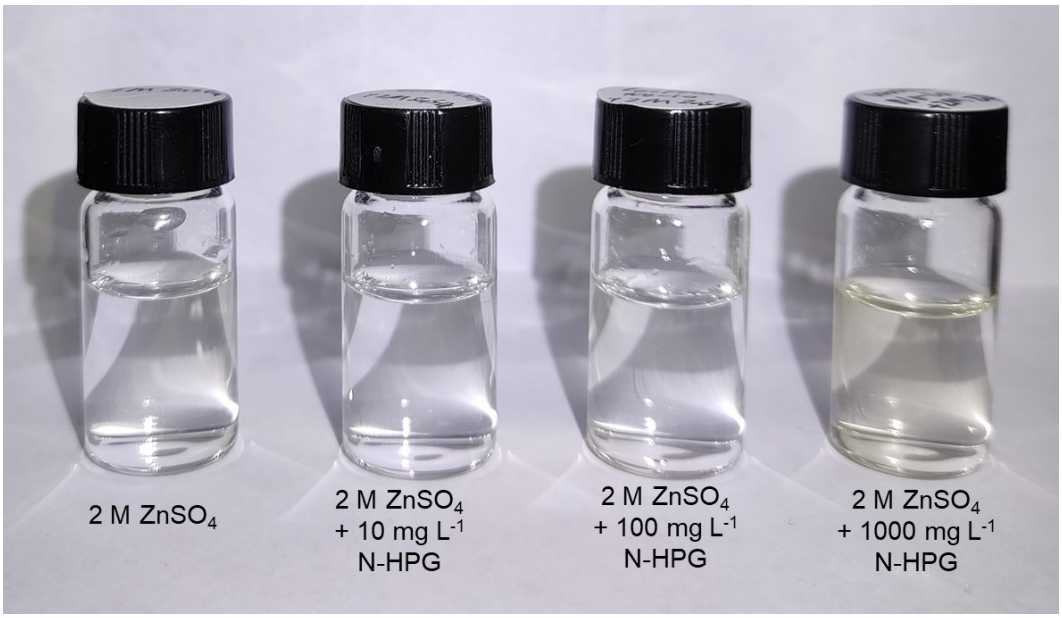

Fig. S3 Optical pictures of N-HPG electrolyte at different concentrations.

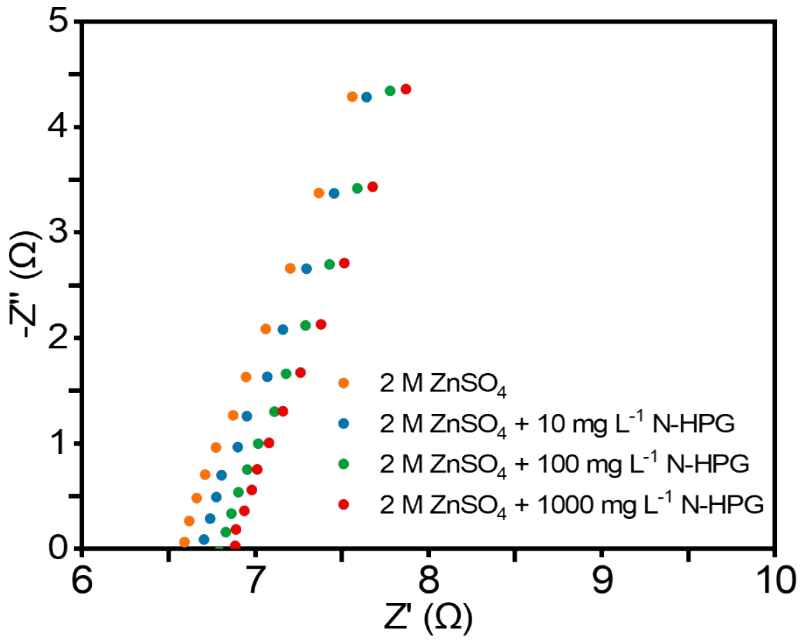

Fig. S4 Magnified high-frequency region of EIS spectra for SS//SS symmetric cells employing various electrolytes

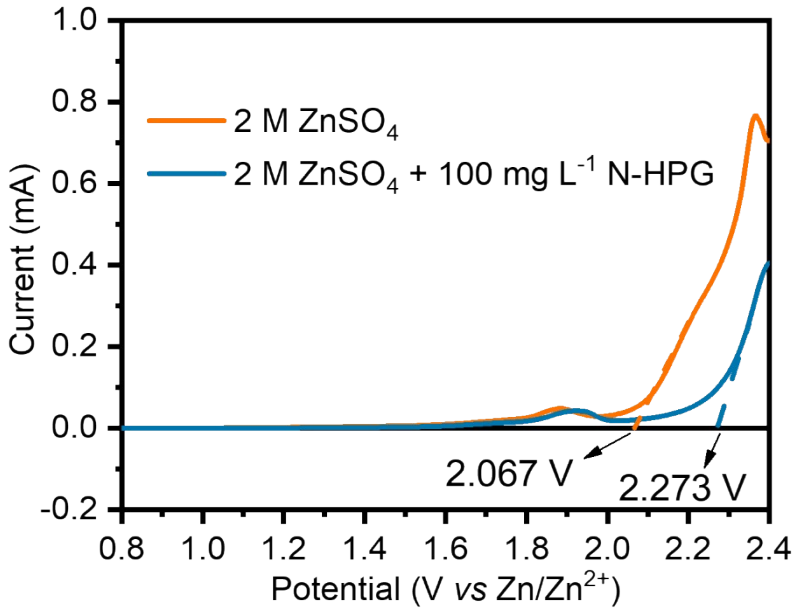

Fig. S5 Oxygen evolution reaction curves in electrolytes with or without N-HPG.

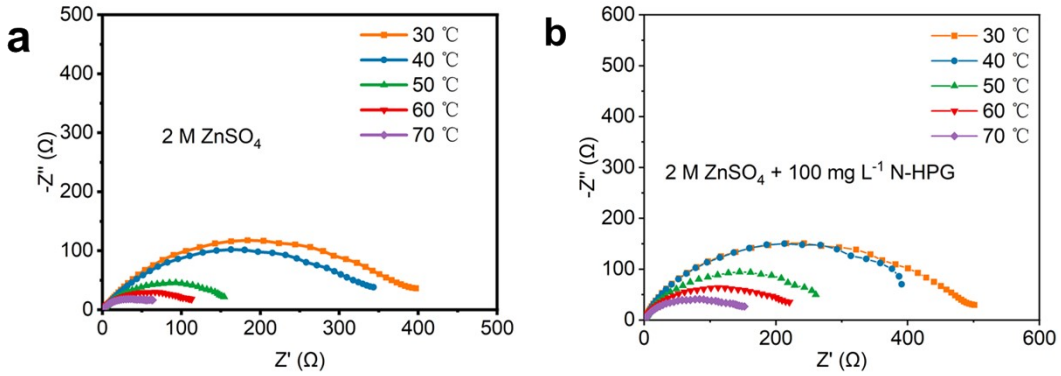

Fig. S6 EIS impedance diagram of (a) 2 M $ZnSO_4$ and (b) 2 M $ZnSO_4$ + 100 mg L^{-1} N-HPG at different temperatures.

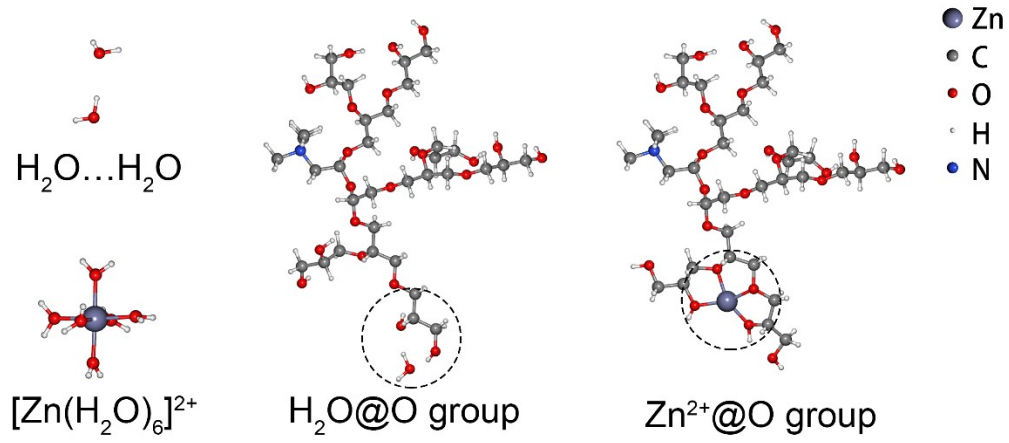

Fig. S7 The schematic illustration of H_2O-H_2O, Zn^{2+}- H_2O, H_2O -O groups and Zn^{2+}-O groups**.**

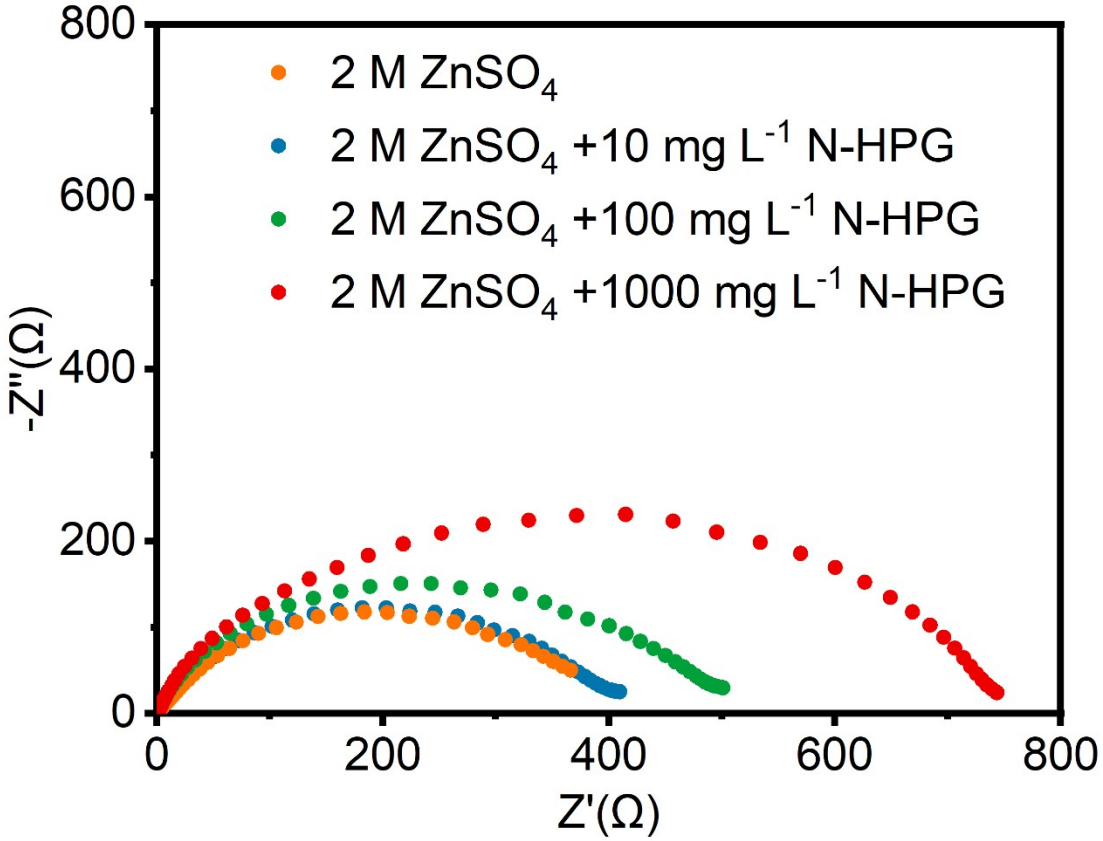

Fig. S8 Nyquist diagram of Zn//Zn symmetric cell in 2 M $ZnSO_4$ with different concentrations of N-HPG.

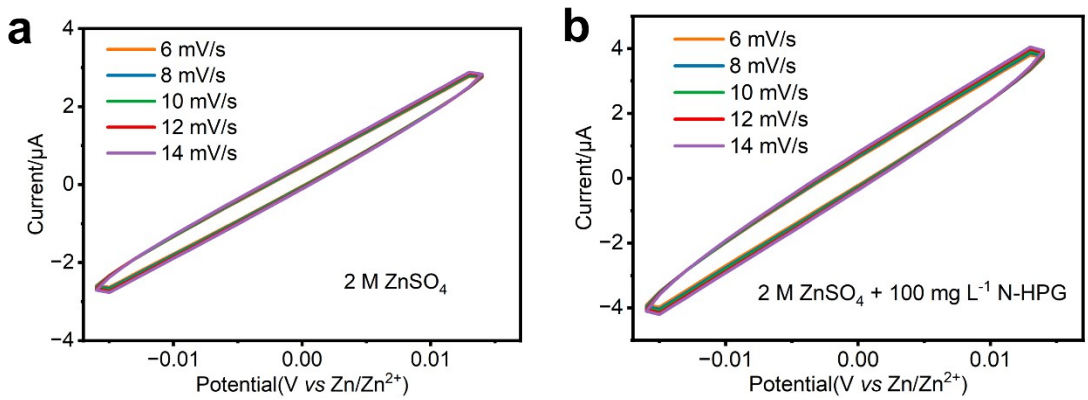

Fig. S9 CV curves of Zn//Zn batteries at different sweep rates in (a) 2 M $ZnSO_4$ and (b) 2 M $ZnSO_4$ + 100 mg L^{-1} N-HPG electrolytes.

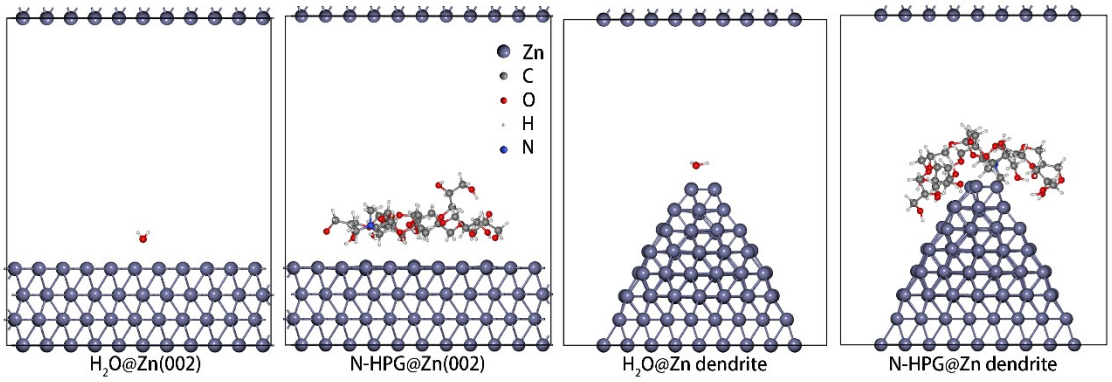

Fig. S10 Under electric field: adsorption configuration of H_2O/N-HPG on the Zn (002) crystal plane and Zn tip.

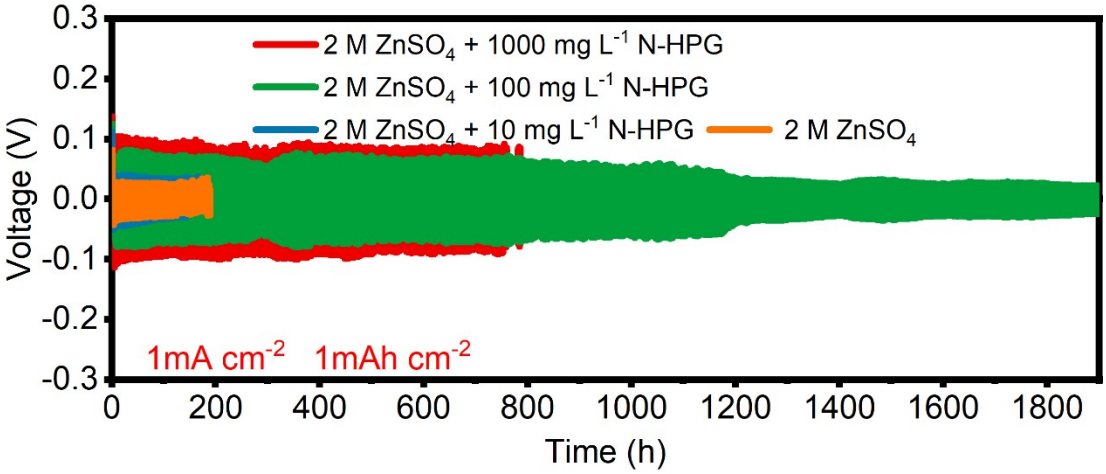

Fig. S11 Long cycle performance of Zn//Zn symmetric cells with different concentrations of N-HPG (1 mA cm^{-2}, 1 mAh cm^{-2}).

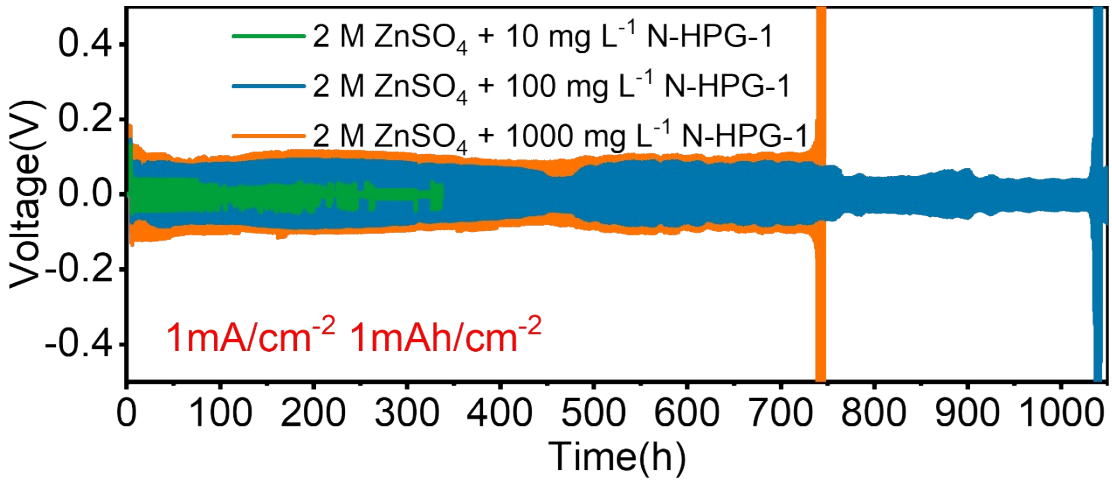

Fig. S12 Long cycle performance of Zn//Zn symmetric cells with different concentrations of N-HPG-1 (1 mA cm^{-2}, 1 mAh cm^{-2}). The additive N-HPG-1 was synthesized by reacting trimethyl epoxypropyl ammonium chloride with 2,3-epoxypropanol at a 1:1 molar ratio, followed by electrochemical testing at varying concentrations in Zn//Zn symmetric cells.

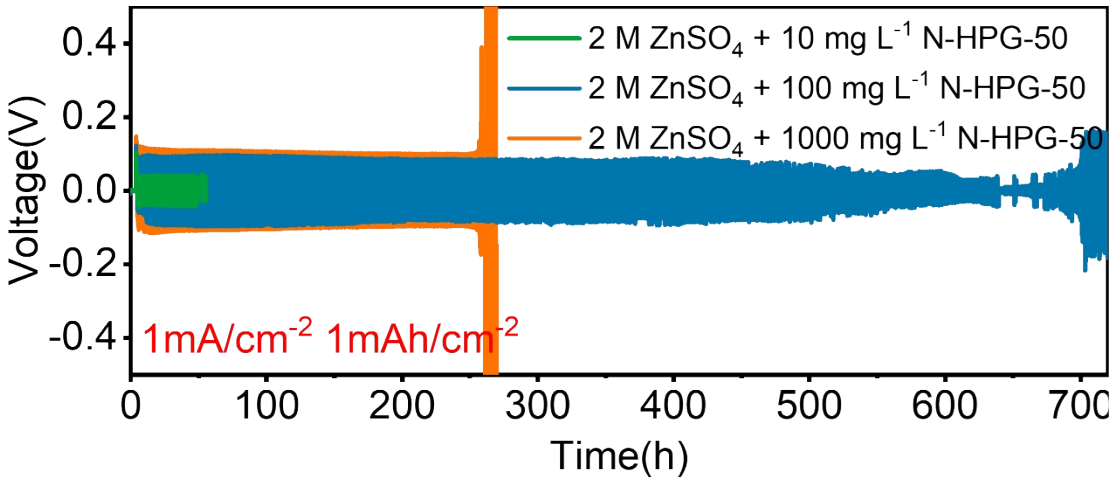

Fig. S13 Long cycle performance of Zn//Zn symmetric cells with different concentrations of N-HPG-50 (1 mA cm^{-2}, 1 mAh cm^{-2}). The additive N-HPG-50 was synthesized by reacting trimethyl epoxypropyl ammonium chloride with 2,3-epoxypropanol at a 1:50 molar ratio, followed by electrochemical testing at varying concentrations in Zn//Zn symmetric cells.

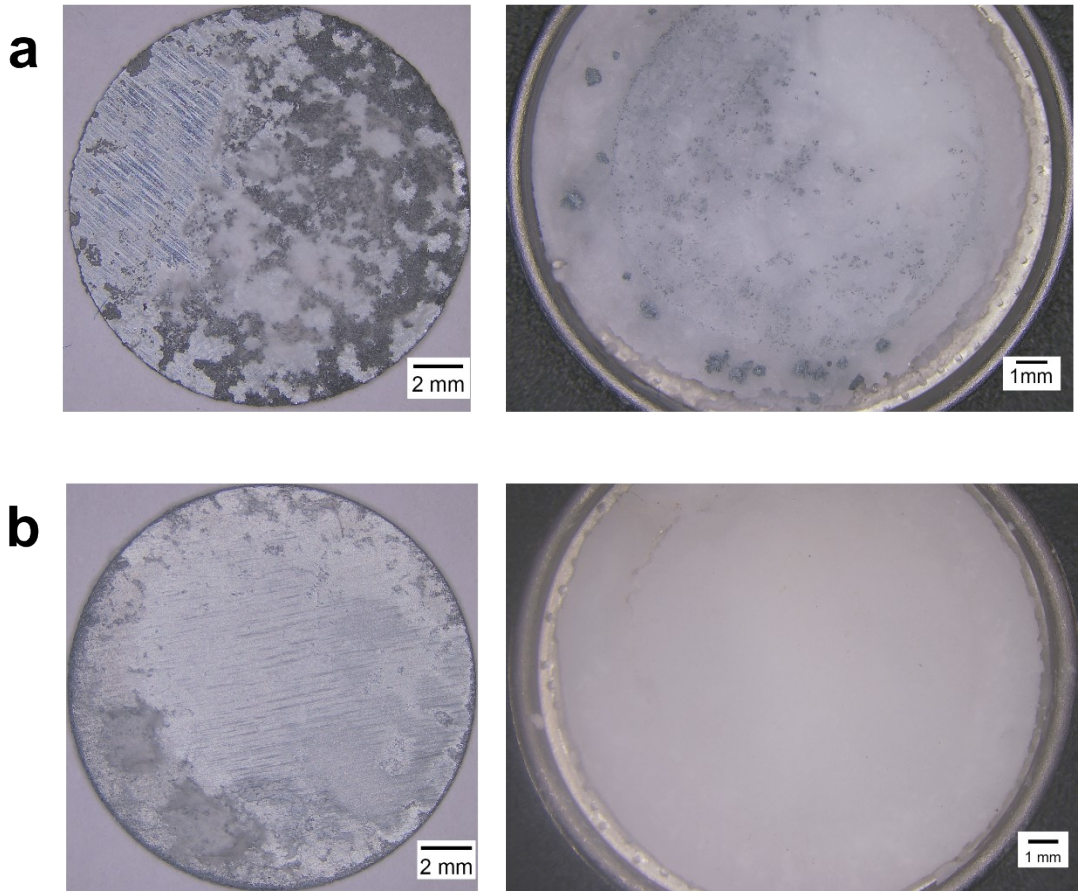

Fig. S14 (a) Optical images of Zn foil (left) and separator (right) after 100 cycles of Zn//Zn symmetric cell cycling in 2 M $ZnSO_4$ electrolyte; (b)Optical images of zinc foil (left) and separator (right) after 100 cycles of Zn//Zn symmetric cell cycling in 2 M $ZnSO_4$ + 100 mg L^{-1} N-HPG electrolyte.

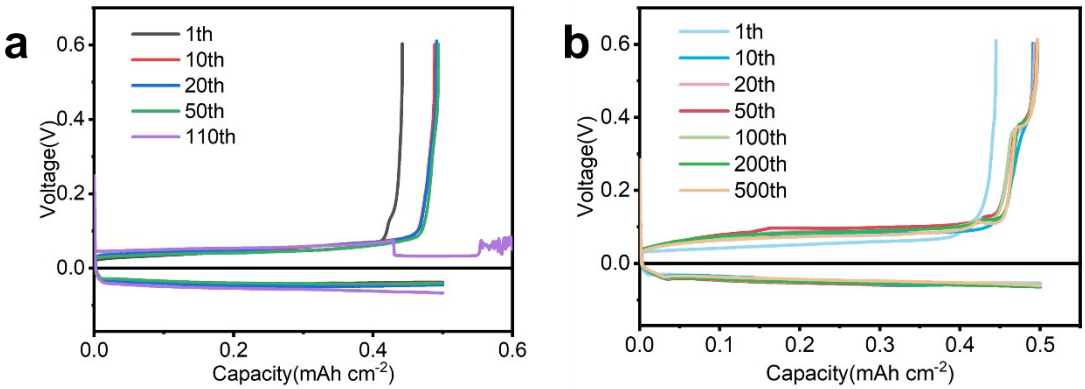

Fig. S15 Corresponding voltage distributions of Zn//Cu cells at different cycles in (a) 2 M $ZnSO_4$ electrolyte and (b) 2 M $ZnSO_4$ + 100 mg L^{-1} N-HPG electrolyte.

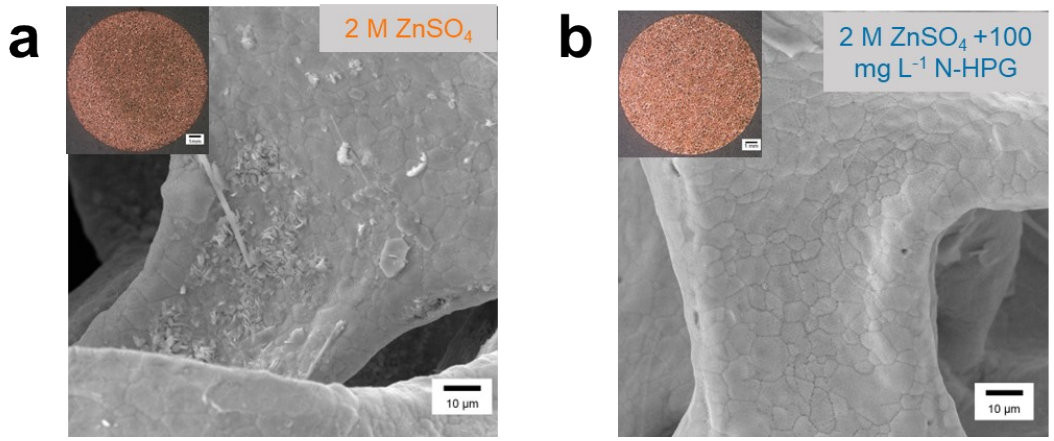

Fig. S16 SEM images of Cu foils after cycling for 100 h in (a) 2 M $ZnSO_4$ and (b) 2 M $ZnSO_4$ + 100 mg L^{-1} N-HPG (Illustrations are optical pictures)

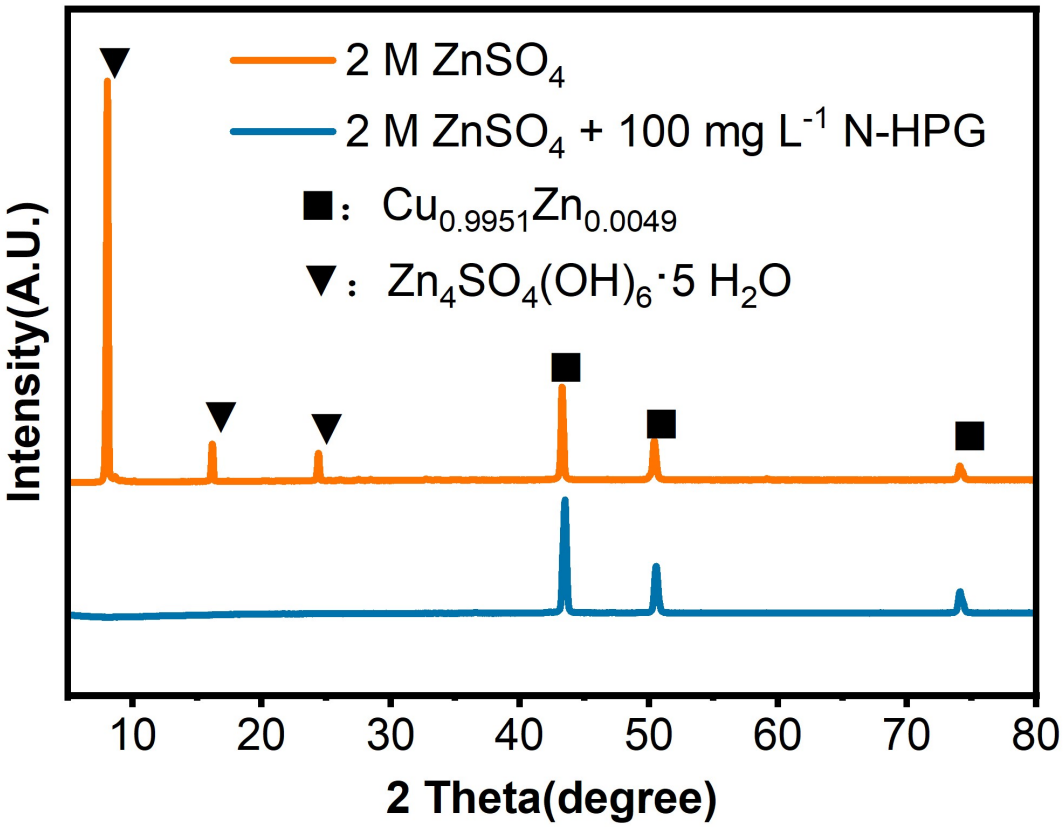

Fig. S17 XRD image of copper foil after 100 h of cycling.

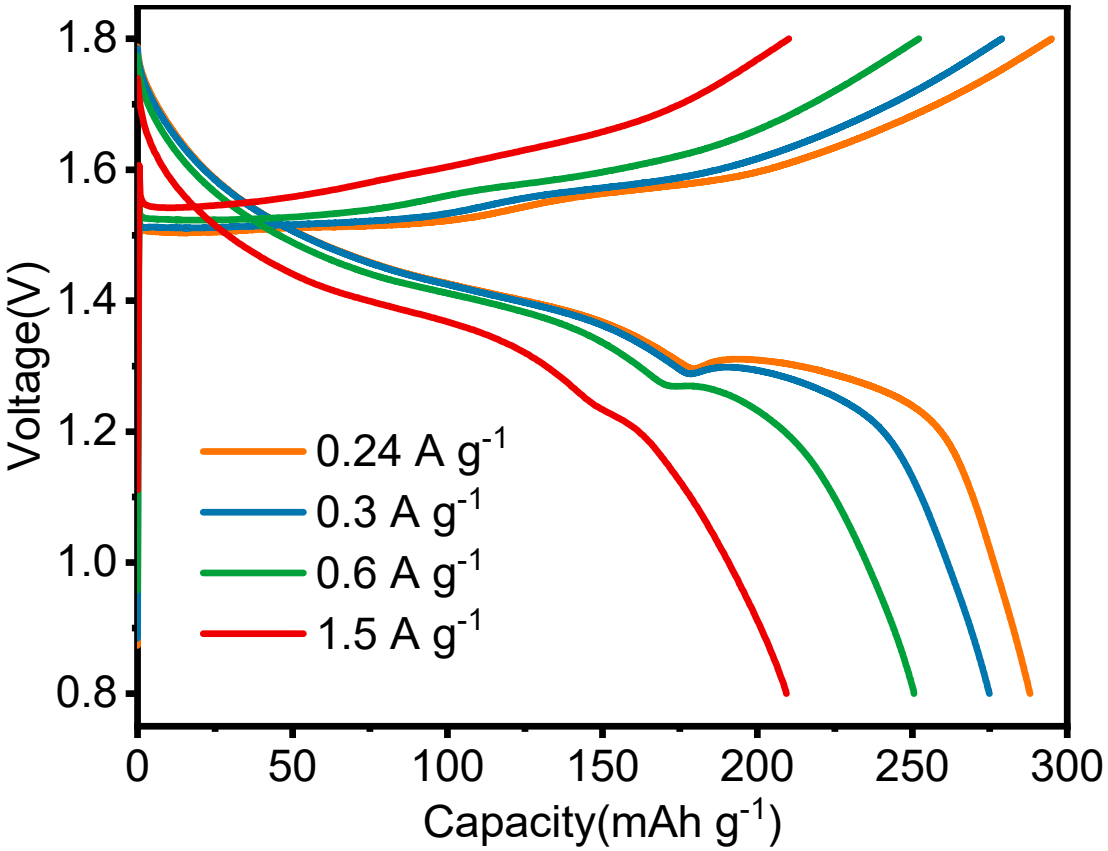

Fig. S18 Voltage-capacity curves for N-HPG containing electrolyte at different current densities

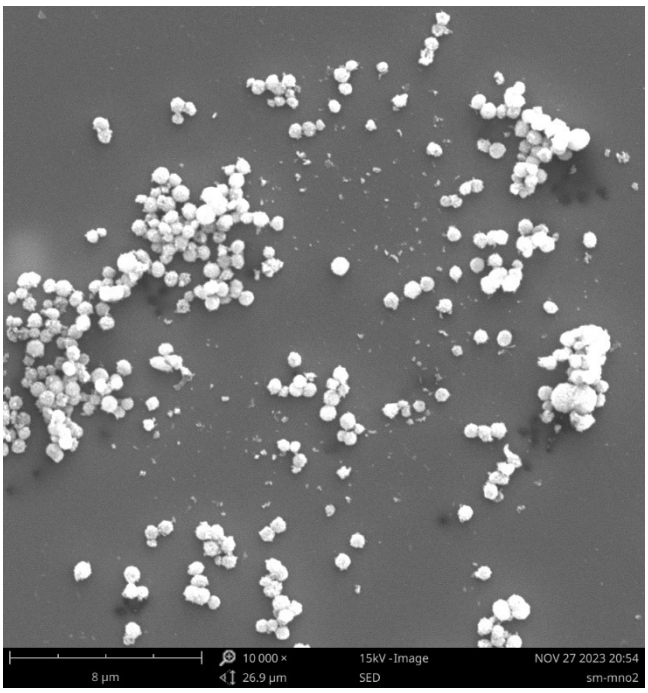

Fig. S19 SEM image of manganese dioxide.

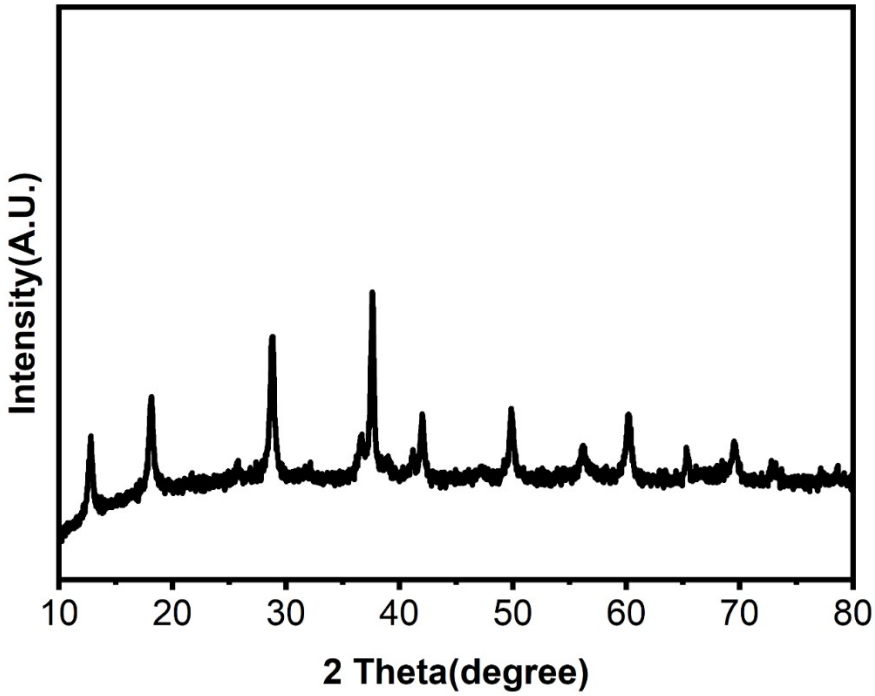

Fig. S20 XRD image of manganese dioxide.

References

1 P. Giannozzi, S. Baroni, N. Bonini, M. Calandra, R. Car, C. Cavazzoni, D. Ceresoli, G. L. Chiarotti, M. Cococcioni and I. Dabo, *J. Phys.: Condens. Matter*, 2009, **21**, 395502.

2 J. P. Perdew, K. Burke and M. Ernzerhof, *Phys. Rev. Lett.*, 1996, **77**, 3865-3868.

3 G. Kresse and D. Joubert, *Physical Review B*, 1999, **59**, 1758-1775.

4 R. Tran, Z. Xu, B. Radhakrishnan, D. Winston, W. Sun, K. A. Persson and S. P. Ong, *Sci. Data*, 2016, **3**, 160080.

5 S. Plimpton, *J. Comput. Phys.*, 1995, **117**, 1-19.

6 S. Schott-Verdugo and H. Gohlke, *Journal of Chemical Information and Modeling*, 2019, **59**, 2522-2528.

7 J. M. Wang, R. M. Wolf, J. W. Caldwell, P. A. Kollman and D. A. Case, *J. Comput. Chem.*, 2004, **25**, 1157-1174.

8 C. S. Babu and C. Lim, *J. Phys. Chem. A*, 2006, **110**, 691-699.

9 W. G. Hoover, *Physical review A*, 1985, **31**, 1695.

10 W. Shinoda, M. Shiga and M. Mikami, *Physical Review B*, 2004, **69**, 134103.